34th Annual International Conference of the IEEE EMBS
San Diego, California USA, 28 August - 1 September, 2012

A Computational Model of a Controllable Needle-Free Jet Injector

Rhys M. J. Williams, N. Catherine Hogan, Poul M. F. Nielsen *Member, IEEE*, Ian W. Hunter, Andrew J. Taberner, *Member, IEEE*

***Abstract*— We present a mathematical model of the dynamics of a previously developed needle-free jet injector (NFJI) that is based upon a servo-controlled Lorentz-force motor. The injector creates a fluid jet that can pierce through the skin and deliver a drug to dermal, subcutaneous and muscular tissue. We use the model to predict the jet speed achieved during an injection. The model simulates the electrical response of the motor coil, the mechanical response of the drug piston and ampoule and the friction incident upon the piston during the time course of the injection. High-speed video measurements of piston movement in response to a step input show that the model predicts piston-tip position during an injection within an RMS error of 287 µm. The corresponding jet speed is predicted to be 180 $m \cdot s^{-1}$ with a maximum overshoot to 205 $m \cdot s^{-1}$.**

I. Introduction

Needle-free jet injectors (NFJIs) typically consist of a fluid-filled ampoule with a small orifice at one end, and a force-generator that pressurizes the fluid. A jet of fluid emerges from the orifice at a speed of up to 200 $m \cdot s^{-1}$ [1]. The fluid jet is able to penetrate the skin and deliver drugs to the dermal, subcutaneous and muscular layers of human and animal tissue. Subsequently, the drugs are absorbed into the interstitial fluid and bloodstream in a process similar to that of the absorption of needle-delivered non-intravenous drugs. NFJIs eliminate the possibility of needle-stick injuries for health professionals and patients and provide a method of drug delivery other than that of needle-and-syringe for needle-phobic patients. NFJI testing has indicated some potential for the technology to reduce the pain and local effects of injection [2].

We have previously demonstrated the performance of a highly controllable needle-free jet injection system using servo-controlled linear Lorentz-force motors [1], [3]. In our system, a position-controlled linear motor [4] propels the piston of a disposable drug ampoule [5] in real-time, thereby achieving quieter and more precise injections than other NFJI systems [6]. However, in this system we are presently unable to directly monitor or control the fluid pressure or jet speed during injections. While the steady-state jet speed can be inferred from the motor position over relatively long time scales (>10 ms), the jet-speed during the initial stages of delivery can only be inferred from a model that describes the dynamic behavior of the injector system.

In this paper we describe a computational model that we have created to capture the physical characteristics of our motor and injection system. We use this model to describe the mechanical and fluidic features of the injector that determine the velocity of the fluid jet over the course of each injection. The model is used to provide insight into how parameters, such as motor velocity and jet speed, vary over time and builds upon the work of Baker et al. [7] and Chen et al. [8].

II. Model

The Lorentz-force motor, ampoule, and fluid that comprise our jet injector can be considered as a coupled electromechanical-fluidic system, as in Fig. 1. Voltage (V) applied to the coil (less the back-emf arising from the motion of the coil y_1) produces a current (I), thereby generating a Lorentz force (F) that drives the mechanical admittance (Y_m) of the drug ampoule, piston and contained fluid [6].

The ampoule piston forms a seal against the fluid via a compliant rubber tip. Additional compliance is contributed by

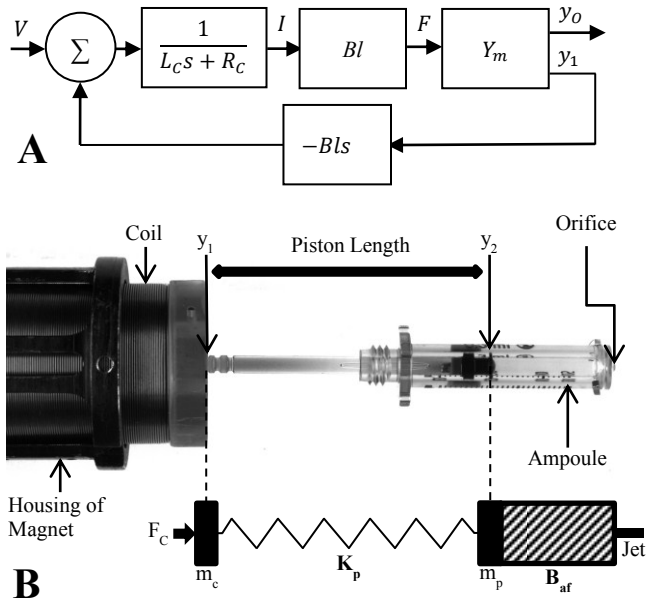

Figure 1 - Block diagram (A) and exploded view (B) of jet injector system

This work was supported in part by the University of Auckland Vice-Chancellor's Strategic Development Fund.

R. M. J. Williams is with the Auckland Bioengineering Institute at the University of Auckland (phone: +64 9 3737 599; fax: +64 9 3677 157; e-mail: rwil267@aucklanduni.ac.nz).

N. C. Hogan is with the Department of Mechanical Engineering at the Massachusetts Institute of Technology (e-mail: hog@mit.edu).

P. M. F. Nielsen is with the Auckland Bioengineering Institute and the Department of Engineering Science at The University of Auckland (e-mail: p.nielsen@auckland.ac.nz).

I. W. Hunter is with the Department of Mechanical Engineering at the Massachusetts Institute of Technology (e-mail: ihunter@mit.edu).

A. J. Taberner is with the Auckland Bioengineering Institute and the Department of Engineering Science at The University of Auckland (e-mail: a.taberner@auckland.ac.nz).

the polycarbonate drug ampoule. Furthermore, significant friction forces act on the rubber piston tip, while the progress of drug through the orifice is opposed by the Bernoulli force [9]. The fluid emerges from the orifice with speed dy_O / dt.

In general, the electrical circuit of a moving-coil Lorentz-force actuator of this type can be approximated by a simple first-order low pass filter (although this assumption ignores the sometimes significant eddy current losses that can be induced in the central core of the magnetic circuit [10]). The measured electrical time-constant of the motor coil was ~1 ms, which is faster than any of the dominant mechanical time constants in the system. The force constant Bl was measured over the stroke of the motor and described by a quadratic function of coil position with Bl = 8.98 N/A ± 1.51 N/A.

The mechanically compliant piston, ampoule and fluid Y_m was modeled as a mass-spring damper system [11]. In this representation, the piston was denoted by a spring of stiffness K_p. The system was described by (1) and (2):

$$\frac{d^2 y_1}{dt^2} = \frac{F - D_C \frac{dy_1}{dt} + K_p(y_2 - y_1 - L_p)}{m_c} \quad (1)$$

where y_1 is the position of the coil, as indicated in Fig. 1, F is the force applied by the motor, D_C is the coil damping coefficient, L_p is the length of the piston and m_c is the mass of the coil.

$$\frac{d^2 y_2}{dt^2} = \frac{-D_P \frac{dy_2}{dt} - K_P(y_2 - y_1 - L_p) - F_{fr} - PA_p}{m_p} \quad (2)$$

where y_2 is the position of the piston tip as indicated in Fig. 1, D_P is the piston damping coefficient, F_{fr} is the friction force, P is the fluid pressure, A_p is the area of the piston, and m_p is the mass of the piston.

To represent the friction force F_{fr} in (2) we made use of the model of Armstrong-Helouvry and Canudas de Wit [12]. This formulation (3) incorporates contributions from Coulomb friction, Stribeck friction and viscous friction.

$$F_{fr} = F_C(1 + (C_{BF} - 1)e^{-C_{TA} abs\left(\frac{dy_2}{dt}\right)}) + C_{VF}\frac{dy_2}{dt} \quad (3)$$

The Coulomb friction (F_C) is defined as the combination of the preload force (F_P), the friction of the seal between the piston and the walls of the ampoule and the Coulomb forward friction force (C_{CFF}), which results from the pressure dependent resistance of the pressure seal (4).

$$F_C = F_P + C_{CFF} P \quad (4)$$

Stribeck friction dominates at low velocities and diminishes as velocity increases. Its effect is incorporated through the breakaway friction force coefficient (C_{BF}) which represents the friction encountered when motion begins, and the transition approximation coefficient (C_{TA}) which indicates when the Stribeck friction is dominated by Coulomb and viscous friction.

Viscous friction was modeled by a viscous friction coefficient (C_{VF}) multiplied by the velocity of the piston tip.

Equation (3) has a discontinuity at y_2 = 0 that can be avoided by defining friction when -0.005 < y_2 < 0.005 as in (5).

$$F_{fr} = \frac{C_F(1 + (C_{BF} - 1)e^{-0.01 C_{TA}}) + 0.01 C_{VF}}{0.01}\frac{dy_2}{dt} \quad (5)$$

The final force in the numerator of (2) arises from the pressure (P) developed in the fluid. The ampoule distends in response to fluid pressure, primarily in the radial direction. This effect was incorporated by defining an effective bulk modulus (B_{af}) that combines the fluid's bulk modulus with the compliance of the ampoule. Measurements from previous experiments and a finite-element model (COSMOS Works) were used to estimate the ampoule distension in response to pressure and (6) was used to calculate the ampoule's effective bulk modulus (B_A).

$$B_A = V_F \frac{dP_F}{dV_F} \quad (6)$$

where P_F is the fluid pressure and V_F is the volume of fluid in the ampoule.

The ampoule bulk modulus was calculated to be 9×10^8 N·m^{-2}. This modulus was combined as a fluid spring in series with the fluid bulk modulus (2.2×10^9 N·m^{-2}) to give a combined bulk modulus value of 6.4×10^8 N·m^{-2} (B_{af}).

The incremental change in pressure was then described [7], [13] by (7) which was solved iteratively.

$$\frac{dP}{dt} = \frac{(B_{af} + P)\frac{dy_2}{dt} - \frac{B_{af} A_O}{A_P}\sqrt{\frac{2P}{\rho}}}{L_p - y_2} \quad (7)$$

where A_O is the area of the orifice, A_P is the area of the piston and ρ is the density of the fluid. This resulting pressure was applied back upon the piston tip as indicated in (2).

Finally, the fluid velocity dy_O / dt through the orifice was found from the Bernoulli Equation (8) as in [7], [8], [13], [14].

$$\frac{dy_O}{dt} = \sqrt{\frac{2P}{\rho}} \quad (8)$$

The parameters used to match the response of the model to the recorded response include both measured parameters and free parameters. All parameters that could be measured were set with values gathered from experiments. The radius of the orifice was set as 96 µm in accordance with measurements that gave the orifice diameter as 193 µm ± 13 µm (n=9). Experimentally-defined and manually-set parameter values are given in Table I and Table II, respectively.

The model was coded in LabVIEW 2011 (National Instruments) using the Control and Simulation Module. A Runge-Kutta-45 algorithm solved the model in 10 s to 20 s.

Data were analyzed using DIAdem 2011 (National Instruments).

In order to validate the model, a step input of 304 V and 25 ms duration was applied to a working prototype of the injector. The coil position was taken from the recordings of the potentiometer position used by the NFJI's control system. The position of the piston tip was imaged using a high-speed camera (Phantom V9), as described in [6]. The movement of leading edge of the piston tip was plotted using a software program (Tracker™) and subsequently synchronized with the potentiometer measurements.

The measured voltage applied to the injector was used as an input to the model and free parameters were adjusted to improve the response (test 1). The test was subsequently repeated on the same injector with model parameters left unchanged (test 2). The RMS error between measured and modeled positions was calculated for each test as a measure of the goodness of fit.

III. Results

A plot of the modeled and measured displacement response from test 1 is shown in Figure 2.

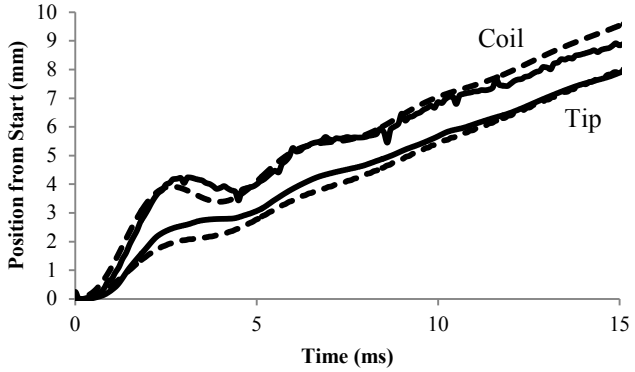

Figure 2 – Model (dashed) and measured (solid) position of the coil and piston tip over 18 ms step response.

TABLE I. Manually Set Parameter Values

Parameter	Value
F_P (Preload Force)	4 N
C_{CFF} (Coulomb Forward Force)	9×10^{-6} m^2
C_{BF} (Breakaway Friction)	1
C_{TA} (Transition Approximation)	5 s·m^{-1}
D_C (Coil Damping Coefficient)	15 N·m·s^{-1}
D_P (Piston Damping Coefficient)	0.01 N·m·s^{-1}
C_{VF} (Viscous Friction Coefficient)	9.36 N·s·m^{-1}

TABLE II. Experimentally Defined Parameter Values

Parameter	Value
R_C (Coil Resistance)	9.67 Ω
K_P (Piston Spring Constant)	200 kN·m^{-1}
M_C (Mass of Coil)	50 g
M_P (Mass of Piston)	0.55 g
A_P (Area of Piston)	1.00×10^{-5} m^2
R_O (Radius of Orifice)	96 µm
L_C (Coil Inductance)	3.5 mH
L_p (Piston Length)	50 mm

Free model parameters were adjusted manually to improve the match between the measured and modeled coil and piston-tip positions. Tables I and II show the final value used for each parameter before performing test 2.

The RMS errors of the two tests are shown in Table III.

TABLE III. RMS Error in Model Fit

Test No.	RMS error of Coil (y_1)	RMS error of Piston Tip (y_2)
1	435 µm	287 µm
2	431 µm	317 µm

Using the best-fit parameters of Table I and the voltage waveform of test 1 as the input, the model was used to compute the resultant jet speed, as shown in Figure 3.

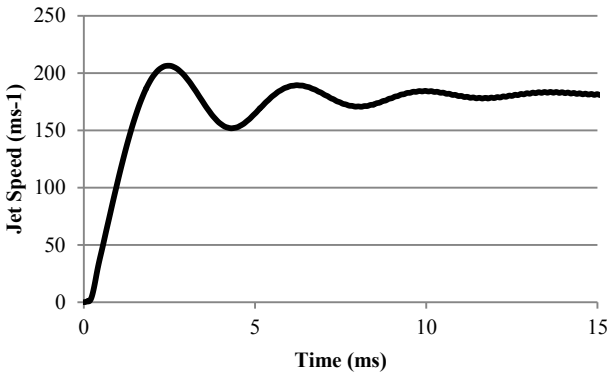

Figure 3 - Jet speed modeled from the first test.

This result indicates a steady-state jet speed of ~180 m·s^{-1} when a step input of 300 V is applied, a value that agrees with measurements from previous experiments [6]. The maximum of the predicted jet speed was 205 m·s^{-1}.

IV. Discussion

Our results (Fig. 2) show that there is good qualitative agreement between the modeled and measured coil and piston-tip positions. The position of the coil and piston tip is estimated with an average RMS error of ~0.4 mm over the time course of a step-response. Although the model may be slightly out of time-alignment with the spring fluctuations of the experimental injection data, the amplitude and length of these fluctuations is similar.

The computational model is able to provide insight into the behavior of the injector when a range of different inputs is applied. Voltage waveforms of arbitrary form can be applied to the model, and the resultant injection speed can be predicted. The model takes between 10 s and 20 s to solve for an 18 ms step response input. The solve time is important as it allows the possibility of future implementation of an automatic model optimization procedure. The rate at which the model results are returned permits quick, iterative analysis of the processes within the NFJI electromechanical system.

The model builds upon previous models of jet injection systems in three ways. Firstly, our model includes the electromechanical properties of the linear Lorentz-force motor used as the pressure source. Secondly, the model

includes terms that describe the compliance of the tip of the piston, and the compliance of the drug ampoule. Thirdly, our model employs a more complete description of the friction components that are present in the system.

The employed friction model separates the sources of friction that arise within the injector. The decoupling of Coulomb friction from Stribeck friction allows the incorporation of more accurate information about the mechanics of the piston-fluid interface. The inclusion of viscous friction allows for future exploration of its contribution to the performance of the injector.

V. Limitations and Future Work

While this model is useful in its current form for exploring the effects of design changes (piston stiffness, ampoule stiffness, orifice diameter) on injector performance, there are several improvements that may enhance the accuracy of model predictions.

To date, we have been unable to directly measure the dynamic changes in jet speed during the time course of injection. Measurement of jet speed requires very high-speed imaging equipment with a field of view of a few millimeters. We have a 72 kHz line-scan camera which, when coupled with the use of particle image velocimetry, will enable a jet speed profile to be measured.

Semi-inductance is a phenomenon whereby the high-frequency impedance of the motor coil has a dependency on ω^n, where $n \approx 0.5$. This effect has long been noted in the loudspeaker literature [15], and has the consequence of decreasing the current rise-time in the motor. The outcome of incorporating semi-inductance in the model will be most apparent during the first 5 ms of current flow.

The piston used in our system has shown evidence of non-linearity in the rubber piston tip. This is thought to be due to the difference in material properties of the polycarbonate piston shaft and the rubber tip. While the shaft deforms elastically, the rubber tip appears to have a non-linear response to the application of force during an injection, particularly at lower forces. Incorporating this effect in the model will greatly affect model predictions during the first 5 ms to 10 ms of injection as this is when the linear approximation is least accurate. The non-linearity will need to be investigated to improve the response during this period.

We have noted that the friction properties of the drug ampoules can change after several injections. The friction model could be informed by a series of experiments that would allow us to experimentally determine the Stribeck, Coulomb and viscous friction elements for each ampoule, and periodically update these parameters over the lifetime of the ampoule.

Finally, we have recently used X-Ray microtomography to measure in detail the tapered geometry of the ampoule orifice. A finite element model is being developed in order to investigate the nature of fluid flow through the orifice, and to explore the extent of geometric changes in orifice dimensions under fluid pressure.

VI. References

[1] Andrew J. Taberner, Nathan B. Ball, N. Catherine Hogan, and Ian W. Hunter, "A Portable Needle-free Jet Injector Based on a Custom High Power-density Voice-coil Actuator," in *Proceedings of the 28th IEEE EMBS Annual International Conference*, New York City, USA, 2006, pp. 5001-5004.

[2] Samir Mitragotri, "Current status and future prospects of needle-free liquid jet injectors," *Nature Reviews Drug Discovery*, vol. 5, no. 7, pp. 543-548, 2006.

[3] Brian D. Hemond, Andrew J. Taberner, N. Catherine Hogan, Brian Crane, and Ian W. Hunter, "Development and Performance of a Controllable Autoloading Needle-Free Jet Injector," *Journal of Medical Devices*, vol. 5, no. 015001, pp. 1-7, March 2011.

[4] N. B. Ball, "An optimized Linear Lorentz-force Actuator for biorobotics and needle-free injection.," Massachusetts Institute of Technology Dept. of Mechanical Engineering, Cambridge, MA, Thesis S. M. 2007.

[5] Injex Pharma Ltd. (2012, March) Injex: The Soft Soft. [Online]. HYPERLINK "http://www.injex.com/" http://www.injex.com/

[6] Andrew J. Taberner, N. Catherine Hogan, and Ian W. Hunter, "Needle-free jet injection using real-time controlled linear Lorentz-force actuators," *Medical Engineering and Physics*, vol. 10, no. 1016, pp. 1-8, December 2011.

[7] Aaron B. Baker and Joan E. Sanders, "Fluid Mechanics Analysis of a Spring-Loaded Jet Injector," *IEEE Transactions on Biomedical Engineering*, vol. 46, no. 2, pp. 235-242, February 1999.

[8] Kal Chen and Hua Zhou, "An experimental study and model validation of pressure in liquid needle-free injection," *International Journal of the Physical Sciences*, vol. 6, no. 7, pp. 1552-1562, April 2011.

[9] Raymond Mulley, *Flow of Industrial Fluids - Theory and Equations*. Boca Raton, FL, United States of America: CRC Press, 2004.

[10] Israel D. Vagner, Boris I. Lembrikov, and Peter Wyder, *Electrodynamics of Magnetoactive Media*. Berlin, Germany: Springer-Verlag, 2004.

[11] Vibrant Technology Inc. (2005, December) Mathematics of a Mass-Spring-Damper System. ME'scopeVES Application Note.

[12] B. Armstrong-Helouvry and C. Canudas de Wit, "Friction Modeling and Compensation," in *The Control Handbook*. Boca Raton: CRC Press, 1996, pp. 1369-1382.

[13] Jeanne C. Stachowiak, Thomas H. Li, Anubhav Arora, Samir Mitragotri, and Daniel A. Fletcher, "Dynamic Control of needle-free jet injection," *Journal of Controlled Release*, vol. 135, no. 2, pp. 104-112, January 2009.

[14] Joy Schramm and Samir Mitragotri, "Transdermal Drug Delivery by Jet Injectors: Energetics of Jet Formation and Penetration," *Pharmaceutical Research*, vol. 19, no. 11, pp. 1673-1679, November 2002.

[15] Knud Thorborg and Claus Futtrup, "Electrodynamic Transducer Model Incorporating Semi-Inductance and Means for Shorting AC Magnetization," *Journal of the Audio Engineering Society*, vol. 59, no. 9, pp. 612-627, September 2011.